Thermal Homogeneity in a Closed Excimer Laser Cavity

Charles J. Knight*
Avco Everett Research Laboratory, Inc., Everett, Massachusetts

Thermal homogeneity in a single-pulse excimer laser cavity is of interest because it directly impacts medium optical quality. This study is primarily oriented toward an XeF* laser in which the cavity is hot (500 K) and is pumped by an e-beam from a cold cathode structure in a vacuum chamber next to the cavity. The foil and support structure are on a vertical wall between these hot and cold zones. In consequence, due to radiative heat transfer, the wall assumes a nonuniform termperature and induces natural convection and thermal inhomogeneity within the cavity. Studies of radiative, conductive, and natural convective heat-transfer processes are summarized which lead to a plausible engineering approach to achieving medium homogeneity of $(\delta\rho/\rho)_{rms} \sim 5\times 10^{-5}$ in the closed XeF* laser cavity.

I. Introduction

THIS paper summarizes part of a thermal design study for a single-pulse laser system. Single-pulse devices have a closed laser cavity with no forced convection. The discussion focuses on an intermediate design stage to delineate the main thermal considerations leading to the final design. Needless to say, many other considerations were involved in defining the overall laser system.

Figure 1 shows the main elements of an excimer laser system that will be of concern here. The cavity gas is pumped by opposed e-beams emitted from a cathode contained in a vacuum chamber on each side of the laser cavity. The cavity and vacuum chambers are separated by walls consisting of a thin foil (1 mil or ~ 25 μm) stretched over a support structure which must be highly transparent to the e-beams to achieve reasonable system efficiency. These walls are typically vertical to allow easy separation of cavity and vacuum chamber for foil repair, etc. The optical direction (between resonator mirrors) is horizontal.

The particular device of primary interest in this paper is an xenon-fluoride (XeF*) laser which produces light output of wavelength $\lambda = 0.35$ μm. The XeF* laser should operate at 450-500 K cavity temperature and about 6 atm pressure for good intrinsic laser efficiency. The device also has a cold cathode e-beam system which is at or near 300 K. The net result of the temperature differential is that the vertical walls defined by the e-beam foils assume a nonuniform temperature distribution which induces natural convection and thermal inhomogeneity within the laser cavity.

The question arose whether it was possible to achieve good cavity medium homogeneity under these circumstances. The specific objective adopted was trying to achieve $(\delta\rho/\rho)_{rms} \leq 5\times 10^{-5}$ as appropriate for the short wavelength laser involved. Many analyses were performed in assessing the feasibility of this goal including nonuniform temperature of the vertical e-beam walls, temperature variation of ceiling and floor along the optical axis, heat losses at the output aperture and primary mirror, and exterior thermal boundary-layer effects. All of these cannot be described in a single paper. The conclusion from these analyses was that the most important effect arises from the optical path-average temperature nonuniformity of the e-beam walls producing an ordered aberration. For that reason as well as limited space, the discussion is limited here to natural convection in a plane normal to the optical axis.

The subsequent discussion will begin with a description of the numerical treatment for two-dimensional natural convection within an enclosure. Thermal modeling and predictions for equal cavity ceiling and floor temperatures will be the subject in Sec. III. Then the utility of thermally grading the boundaries in an attempt to stably stratify the cavity gas is assessed. The studies in Secs. III and IV both involve a stainless steel foil support structure (the intermediate design), and they show that adequate cavity medium homogeneity cannot be expected with such a low thermal conductivity material. The final foil support design, described in Sec. V, employs copper.

Received Feb. 8, 1981; presented as Paper 81-1132 at the AIAA 16th Thermophysics Conference, Palo Alto, Calif., June 23-25, 1981; revision received July 2, 1982.

*Principal Research Scientist. Member AIAA.

II. The Boussinesq Approximation

Natural convection of gas within the closed laser cavity will be analyzed on the basis of the Boussinesq approximation.[1] What this means basically is that the gas is treated as having constant density except for generation of buoyancy forces, and the density differences leading to buoyancy are due to temperature differences only. For laminar flow this leads to the following system of equations expressing conservation of mass, momentum, and energy:

$$\mathrm{div}(V) = 0$$

$$\frac{\partial V}{\partial t} + V\cdot\mathrm{grad}(V) + \mathrm{grad}\left(\frac{\delta p}{\rho_0}\right) = g\frac{\delta T}{T_0}e_y + \nu_0\nabla^2 V$$

$$\frac{\partial \delta T}{\partial t} + V\cdot\mathrm{grad}(\delta T) = \alpha_0\nabla^2(\delta T) \qquad (1)$$

where subscript zero denotes some mean cavity condition (e.g., 6 atm and 500 K), $\delta T = T - T_0$ is a temperature deviation, δp the deviation in pressure from the local hydrostatic value, g the acceleration of gravity, ν_0 the kinematic viscosity, and α_0 the thermal diffusivity. The Boussinesq approximation is valid if some measure of the thermal nonuniformity ΔT is small compared to the mean cavity temperature T_0. Even though the theory assumes small $\Delta T/T_0$, it is fundamentally nonlinear if convective heat transfer dominates thermal diffusion in the gas.

It will be convenient to introduce nondimensional variables and in the process arrive at parameters which define the nature of a particular problem. Set $\tau = Ut/H$, $\xi = x/H$, $v = V/U$, $\pi = \delta p/\rho_0 U^2$, and $\theta = (T - T_0)/\Delta T$ to arrive at

$$\mathrm{div}(v) = 0$$

$$\frac{\partial v}{\partial \tau} + v\cdot\mathrm{grad}(v) + \mathrm{grad}(\pi) = \left(\frac{gH\Delta T}{U^2 T_0}\right)\theta e_y + \left(\frac{\nu_0}{UH}\right)\nabla^2 v$$

$$\frac{\partial \theta}{\partial \tau} + v\cdot\mathrm{grad}(\theta) = \left(\frac{\alpha_0}{UH}\right)\nabla^2\theta \qquad (2)$$

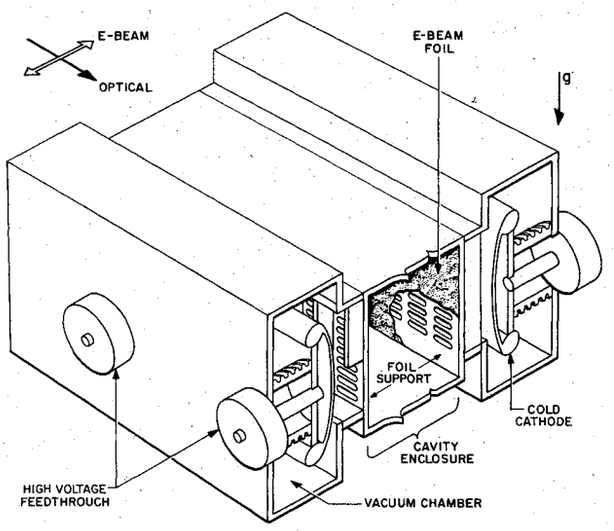

Fig. 1 Single-pulse excimer laser configuration.

The length scale H is most meaningfully taken to be the height of the cavity enclosure. The most meaningful velocity scale for the strong convection situation of interest here is $U_B=\sqrt{gH\Delta T/T_0}$, which is proportional to the speed achieved by an element of gas ΔT hotter than its ambient surroundings after starting from rest and rising vertically a distance H. Then the basic nondimensional parameters involved in Eq. (2) are

$$Gr=gH^3\Delta T/T_0\nu_0^2 \qquad \text{(Grashof number)}$$

$$Pr=\nu_0/\alpha_0 \qquad \text{(Prandtl number)} \tag{3}$$

Note that the normalizing time scale, $t_B=H/U_B$, will increase as ΔT decreases.

The Grashof numbers involved here will be large. This implies nonlinear flow and necessitates a numerical treatment. Attention is restricted to two-dimensional transient motion in a plane normal to the optical axis, for reasons discussed in the preceding section. In that case it is preferable to introduce an alternate set of dependent variables.[2] The two-dimensional continuity equation implies the existence of a stream function ψ such that

$$u=-\frac{\partial\psi}{\partial\eta}, \qquad v=\frac{\partial\psi}{\partial\xi} \tag{4}$$

where η measures vertical distance. Also, pressure can be eliminated by cross differentiating and subtracting the momentum equations. The net result is to replace Eq. (2) by

$$\frac{\partial^2\psi}{\partial\xi^2}+\frac{\partial^2\psi}{\partial\eta^2}=\omega$$

$$\frac{\partial\omega}{\partial\tau}+\frac{\partial}{\partial\eta}(u\omega)+\frac{\partial}{\partial\eta}(v\omega)=\frac{\partial\theta}{\partial\xi}+\frac{1}{\sqrt{Gr}}\left(\frac{\partial^2\omega}{\partial\xi^2}+\frac{\partial^2\omega}{\partial\eta^2}\right)$$

$$\frac{\partial\theta}{\partial\tau}+\frac{\partial}{\partial\xi}(u\theta)+\frac{\partial}{\partial\eta}(v\theta)=\frac{}{Pr\sqrt{Gr}}\left(\frac{\partial^2\theta}{\partial\xi^2}+\frac{\partial^2\theta}{\partial\eta^2}\right) \tag{5}$$

where $\omega=\partial v/\partial\xi-\partial u/\partial\eta$ is the ζ-component of the vorticity vector. The last two equations have been written in conservative form using the continuity equation because that is the form used in the numerical algorithm. Note that $\sqrt{Gr}$ plays a role analogous to the Reynolds number in forced convection flows and that a large Grashof number means the diffusion terms can only be important in narrow "boundary-layer" regions.

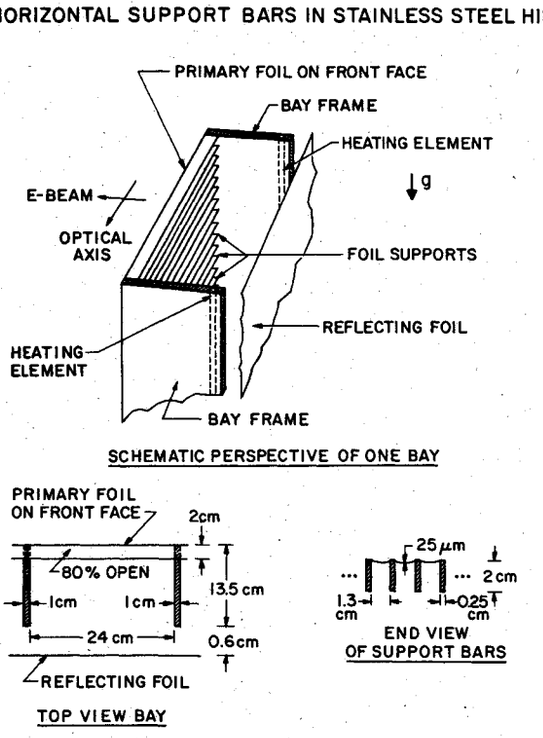

Fig. 2 Schematic of intermediate foil support design.

Efficient numerical solution of Eqs. (5) represents a demanding task even in a simple domain such as the rectangular region considered in this paper. The algorithm used here[3] employs fast Fourier transform (FFT) techniques to solve the Poisson equation for ψ and implicit Peaceman-Rachford update of the vorticity and thermal transport equations. To avoid an instability encountered in previous treatments with implicit methods, the update of vorticity at boundary and interior grid points was coupled. Briley[4] had previously concluded the instability could be avoided in that way. The implicit treatment gives significant gain in computational economy compared to an explicit treatment.[3]

There are two more points that should be noted. The Boussinesq equations derived above assume laminar flow. In typical situations[5] laminar conditions in a natural convection flow can be expected for $Ra<10^9$-10^{10}, where the Rayleigh number $Ra=Pr\cdot Gr$. There are exceptions such as a cold gas layer flowing over a hot floor where transition can occur for smaller values of Ra, but the numbers given are adequate for this discussion. The estimated values of Rayleigh number for the laser cavity considered here, which are discussed later, are in the range 10^7-10^8 or so. Thus, solutions of the laminar Boussinesq equations can be expected to give a representative picture of the flow in the cavity.

The other point is that the boundary-layer thickness at these high Rayleigh numbers (roughly $Ra^{-1/4}$) is comparable to the grid spacing that can be afforded. This implies numerical diffusion comparable to the physical diffusion. Thus, the numerical results are qualitatively correct only. This statement should not be misconstrued, however. The largest error is in the heat-transfer rates at boundaries, not in the internal isotherm distributions which primarily determine optical homogeneity.

III. Analysis for an Intermediate Design

The foil support design shown in Fig. 2 will be the prime consideration of this paper. It is a complicated structure consisting of bays along the optical axis defined by vertical frames which transfer the load to the vacuum chamber.

Horizontal bars between the frames support the primary e-beam foil, which separates cavity gas and vacuum. The laser cavity is to the left and the e-beam cathode and surrounding structure are to the right in the perspective view. Rod heating elements are imbedded in each bay frame to adjust the temperature distribution on the vertical e-beam walls. At this intermediate design stage, the entire foil support structure was to be made of stainless steel.

In this section attention will be restricted to the case of equal bay frame and cavity floor and ceiling temperatures. The more general situation will be addressd in the following section. Modeling the foil and foil support system will require consideration of radiative and conductive heat transfer. This is done with an idealized treatment meant primarily to demonstrate plausibility and will be followed by a numerical calculation of natural convection induced within the cavity. Convective heat-transfer effects on foil temperature are overlooked to decouple the problems.

Radiative Heat Loss through e-Beam Foil

Cavity thermal inhomogeneity arises from radiative heat transfer between the e-beam wall and cold cathode, so a prime objective is reducing the loss rate. To illustrate the necessity of this, note that equal radiative heat-transfer rates on the two sides of the primary foil involves

$$T_f = [(T_c^4 + T_a^4)/2]^{1/4} \tag{6}$$

For a cavity temperature $T_c = 500$ K and an ambient temperature $T_a = 300$ K, this would imply a primary e-beam foil temperature $T_f = 433$ K. Although heat conduction through the foil and support bars would reduce this temperature defect, it is fairly evident that improvement is necessary to achieve the requisite cavity medium homogeneity ($\delta T_{\text{rms}} \lesssim 0.025$ K).

Decreasing the emissivity of the primary foil and support structure on the vacuum side is relatively ineffective because they form a cavity which behaves approximately as a perfect blackbody even for small emissivity.[6] This is true because radiation can be expected to experience many bounces, on average, in the relatively deep intrabar space. Another alternative is followed in this design: placing a secondary foil within the vacuum chamber and before the cold cathode to act as a radiation shield. The effectiveness of such a radiation shield will first be assessed without regard to conduction. The support structure will be treated as if it were infinitesimally thin for the purpose of this discussion.

Consider the first of the two configurations depicted in Fig. 3, where subscript f is associated with the primary foil and subscript r with the secondary reflecting foil. If the foils are considered to be infinite and the bay frames in Fig. 2 are perfect reflectors, the following relations are representative under radiative equilibrium conditions:

$$\begin{aligned} \sigma(T_c^4 - T_f^4) &= \epsilon_{r_c}\sigma(T_f^4 - T_r^4) \\ \epsilon_{r_c}\sigma(T_f^4 - T_r^4) &= \epsilon_{r_a}\sigma(T_r^4 - T_a^4) \end{aligned} \tag{7}$$

where $\sigma = 5.67 \times 10^{-12}$ W/cm^2·K^4 is the Stefan-Boltzmann constant. After manipulation, these relations lead to

$$T_c^4 - T_f^4 = (T_c^4 - T_a^4) \Big/ \left(1 + \frac{1}{\epsilon_{r_c}} + \frac{1}{\epsilon_{r_a}}\right) \tag{8}$$

To get the primary foil temperature as close to the mean cavity temperature as possible, and hence reduce cavity thermal inhomogeneity, the values of ϵ_{r_c} and ϵ_{r_a} should be chosen to be very small. In other words, the secondary foil should be highly reflective on *both* sides.

The emissivity of the primary foil is generally going to be less than one, and this is significant primarily on the cavity side where there are no support bars. To assess the effect, consider the second configuration in Fig. 3. Radiative flux balance relations for this situation can be manipulated to find

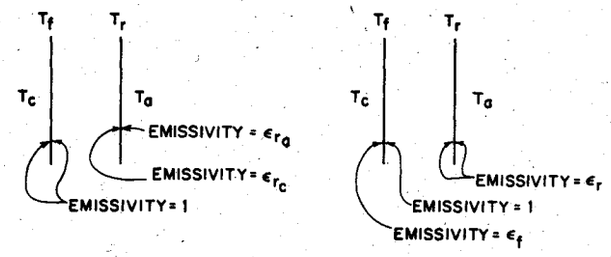

Fig. 3 Thermal radiation shielding using a secondary deflecting foil.

$$T_c^4 - T_f^4 = (T_c^4 - T_a^4) \Big/ \left(1 + 2\frac{\epsilon_f}{\epsilon_r}\right) \tag{9}$$

The value of ϵ_f/ϵ_r should clearly be as large as possible. In other words, the reflectivity of the primary foil should be low and the reflectivity of the secondary foil should be high.

For the purpose of this discussion the primary foil can be assumed to be made of titanium. Titanium should react with the fluorine in the laser gas mixture, and this would presumably alter its surface properties in a manner analogous to exposure to oxygen at high temperature. Oxidized titanium has an emissivity of 0.2-0.5 at frequencies corresponding to a 500 K blackbody. By coating a Kapton foil with a thin layer of aluminum or other metals, it is also reasonable to expect 96-98% reflectivity for the secondary foil. Values of T_f are given in Table 1 for $T_a = 300$ K and $T_c = 500$ K to illustrate the effect of the two foil emissivities. The reduction in vertical wall temperature defect that can be achieved with a secondary reflecting foil is impressive.

There is a tendency to try introducing another reflecting foil for further improvement. The main factor that argues against this is that a fraction of the e-beam will be absorbed by each successive foil, decreasing the electrical efficiency of the laser system. Only a single reflecting foil in each vacuum chamber will be considered here.

Thermal Nonuniformity of Vertical Walls

Now consider combined radiation and conduction to determine the vertical wall temperature distribution. The bay frames are assumed to be perfect reflectors, and the power input from the heating elements in Fig. 2 is assumed to be such that the bay frames and the ends of the support bars are at the same temperature as the floor and ceiling of the cavity T_c. To derive a steady-state conduction equation, consider the end view of the support bars in Fig. 2. The primary foil has

Table 1 Primary foil temperation for radiation only ($T_f \sim$ K)

	$1-\epsilon_r$			
ϵ_f	1	0.98	0.96	0.90
1	500	498.9	497.9	494.7
0.5	500	497.9	495.8	489.8
0.2	500	494.7	489.8	476.7
0.1	500	489.8	480.8	458.9

Table 2 Combined radiation and conduction for intermediate foil-wall design

	ϵ_f			
	1	0.5	0.2	0.1
K	25.3	12.9	5.37	2.87
$T_c - T_w \sim$ K	0.98	1.50	2.21	2.64

negligible thermal mass, so integration over the foil and foil support region leads to

$$\alpha_s h_s k_s \frac{d^2 T_s}{dz^2} + \dot{Q}_R = 0 \tag{10}$$

where $\alpha_s = 0.2$ is the solidity of the foil support structure, $h_s = 2$ cm is the depth of the support bars, k_s is the thermal conductivity, T_s is the local support bar temperature, z is in the optical direction, and $\dot{Q}_R$ is the net radiant power flux. In all cases subscript s will refer to the foil support bars. Note that heat flows from the foil to support bars if $\dot{Q}_R > 0$.

The foil temperature is not immediately obvious. Without any cavity radiation it would be lower than the local value of T_s. On the other hand, if radiation dominates conduction through the foil there is reason to believe the foil temperature will be between T_c and T_s due to view-factor considerations. Here it will be assumed that $T_f = T_s$. This can be approached, if by no other means, through use of a high conductivity foil material such as aluminum. With $T_f = T_s$ it is reasonable to set

$$\dot{Q}_R = \epsilon_f \sigma (T_c^4 - T_s^4) - \epsilon_r \sigma (T_s^4 - T_r^4) \tag{11}$$

Also, $T_r^4 = (T_s^4 + T_a^4)/2$ with the same emissivity on both sides of the reflecting foil. The situation modeled corresponds to the second configuration in Fig. 3.

This differential model is nonlinear and will be avoided. Since T_s near T_c is expected for conditions of interest, consider linearizing the expression for $\dot{Q}_R$ for small $T_s' = T_s - T_c$ to find

$$\dot{Q}_R \sim -\tfrac{1}{2}\epsilon_r \sigma (T_c^4 - T_a^4) - (4\epsilon_f + 2\epsilon_r)\sigma T_c^3 T_s' \tag{12}$$

The linearized form is quite accurate for $\epsilon_f \gtrsim 0$ and $\epsilon_r \sim 0.03$ as may be seen by considering the case of $k_s = 0$ and comparing with Table 1.

With the bay frames at uniform temperature T_c, the solution of Eq. (10) should satisfy $T_s = T_c$ on $z = 0$ and L_s where $L_s \approx 24$ cm is the distance between bay frames. Thus, the solution to the linearized problem is

$$\theta_s = 1 - \cosh\left[\left(\frac{z}{L_s} - \frac{1}{2}\right)\sqrt{K}\right] \Big/ \cosh\left(\frac{1}{2}\sqrt{K}\right) \tag{13a}$$

with

$$\theta_s = (8\epsilon_f + 4\epsilon_r) T_c^3 (T_c - T_s) / \epsilon_r (T_c^4 - T_a^4) \tag{13b}$$

$$K = (4\epsilon_f + 2\epsilon_r)\sigma T_c^3 L_s^2 / \alpha_s h_s k_s \tag{13c}$$

For $K \to \infty$ radiation dominates conduction and $\theta_s \sim 1$ except in the immediate vicinity of the bay frames. This defines the meaning of the normalization for temperature deviation in Eq. (13b). The other extreme of $K \to 0$ leads to

$$T_s' = \epsilon_r \sigma (T_c^4 - T_a^4) z(1 - z) / 4\alpha_s h_s k_s \tag{14}$$

as expected for conduction with a uniformly distributed energy loss of $\epsilon_r \sigma (T_c^4 - T_a^4)/2$.

The optical path-average temperature of the vertical walls T_w will be needed to analyze cavity gas motion in a plane normal to the optical axis. Using the result in Eq. (13a)

$$\theta_w = \frac{1}{L_s}\int_0^{L_s} \theta_s dz = 1 - \frac{2}{\sqrt{K}} \tanh\left(\frac{\sqrt{K}}{2}\right) \tag{15}$$

and the corresponding value of T_w follows from the normalization in Eq. (13b). For the situation considered in this subsection T_w will be independent of the vertical coordinate and it will be lower than the ceiling and floor temperature T_c. Typical values are given in Table 2 for the case of a stainless steel foil support structure with $T_c = 500$ K, $T_a = 300$ K, and $\epsilon_r = 0.03$. Note that radiation tends to dominate conduction with this design due to the low conductivity of stainless steel.

Numerical Simulation without Thermal Grading

Convective heat transfer would actually alter the foil temperature somewhat, but this will be overlooked to decouple vertical wall temperature from determination of the natural convection field in the cavity gas. The nondimensional gas temperature $\theta = (T - T_w)/(T_c - T_w)$, entering Eqs. (5), will be used for the numerical simulation. That is, $\theta = 1$ on the floor and ceiling and $\theta = 0$ on the vertical walls of a square two-dimensional enclosure. The nondimensional groups discussed in Sec. II are taken to be $Gr = 4 \times 10^7$ and $Pr = \frac{2}{3}$, corresponding to neon at 6 atm and 500 K, $H = 60$ cm, and $\epsilon_f \approx 0.2$ in Table 2. The gas is taken to be at rest and at the mean boundary temperature (i.e., $\theta = \frac{1}{2}$) for $\tau = 0$. This does not necessarily represent the experimental condition in which gas is rapidly injected into an evacuated laser cavity, having been heated in a pebble-bed heat exchanger. On the other hand, it is adequate to assess the time to steady-state natural convection. In operation, initial transients would be allowed to decay before firing the laser to achieve the best possible medium homogeneity.

The evolution of the flowfield is displayed by the sequence of contour plots in Fig. 4. Convective motion is predominantly initiated by the temperature defect on the vertical walls, but the hot floor begins to assert itself soon thereafter. For $t/t_B \gtrsim 10$, where t_B is defined after Eq. (3), the convection pattern is essentially the same as if there were a fairly small-width hot spot on the floor.[3,5] For $t/t_B \gtrsim 60$ the hot ceiling also asserts itself in a manner that can be seen in the last three contour plots in Fig. 4. At earlier times the flowfield was symmetrical about $\xi = \frac{1}{2}$, but at late times the upper 30-40% of the central plume oscillates about the cavity centerline. A plausible interpretation is that a hot layer has formed below the ceiling and caused the plume of cooler gas to be unstable due to its negative buoyancy in that layer.

The plume instability also has an effect on heat transfer at late time, as seen in Fig. 5. The Nusselt numbers in the upper plot are numerical approximations to

$$\dot{Q}_{\text{in}} = \int_0^1 \left[\frac{\partial \theta}{\partial \eta}\right]_{\eta=0}^{\eta=1} d\xi$$

$$\dot{Q}_{\text{out}} = -\int_0^1 \left[\frac{\partial \theta}{\partial \xi}\right]_{\xi=0}^{\xi=1} d\eta \tag{16}$$

where ξ is horizontal and η is vertical. The fluctuations in $QFIN$ ($\approx \dot{Q}_{\text{in}}$) arise at the ceiling as the plume oscillates back and forth. Thermal equilibrium, in an oscillatory sense, has been well established by the end of this numerical simulation.

A measure of cavity medium optical homogeneity, $\delta\theta_{\text{rms}}$, is also given in Fig. 5. Here

$$\left(\frac{\delta\rho}{\rho}\right)_{\text{rms}} \sim \left(\frac{\delta T}{T}\right)_{\text{rms}} = \left(\frac{T_c - T_w}{T_c}\right)\delta\theta_{\text{rms}} \tag{17}$$

and the correction for astigmatism or cylindrical focus is in the vertical direction. From Fig. 5, $\delta\theta_{\text{rms}} \approx 0.14$ and so $(\delta\rho/\rho)_{\text{rms}} \sim 6 \times 10^{-4}$ within a minute or so after the simulation begins. The time follows since $t_B \approx 3.8$ s for the conditions assumed. The isotherm distributions in Fig. 4 indicate that it is highly improbable that the required medium homogeneity is achieved in any significant subdivision of the cavity for the case considered in this section.

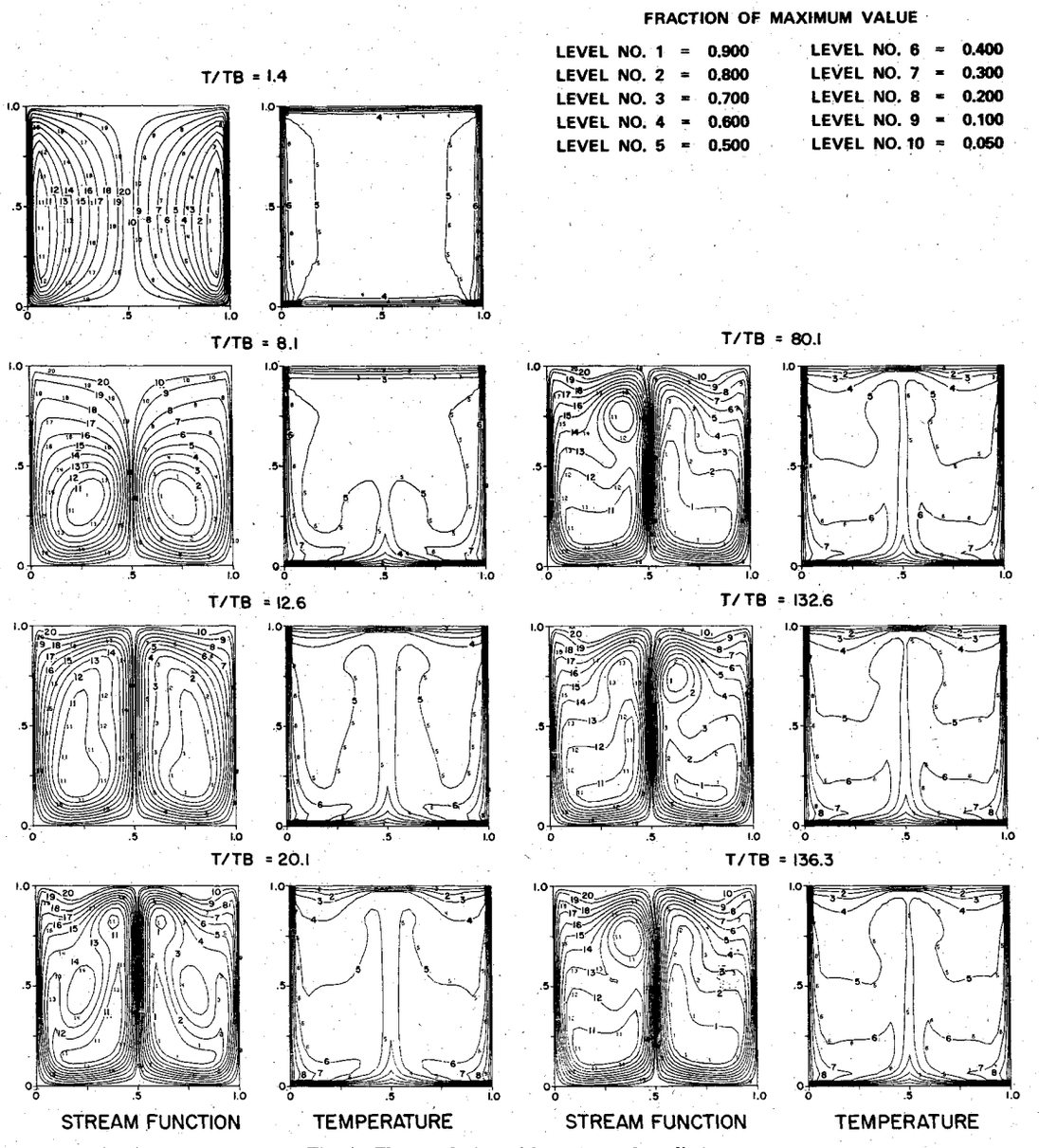

Fig. 4 Flow evolution with no thermal grading.

IV. Adjustable Floor, Ceiling, and Bay Frame Temperatures

The medium homogeneity predicted for the design in the previous section is an order of magnitude larger than the goal of $(\delta\rho/\rho)_{\text{rms}} \sim 5 \times 10^{-5}$. Options that might improve cavity medium homogeneity are as follows:

1) Many closely spaced fins can be placed on the floor and ceiling which are aligned with the flow transverse to the optical axis. This has the aim of increasing the heated surface area to which the gas is exposed. Modeling fins on the floor and ceiling for use in the numerical algorithm is not trivial. Moreover, fins are not necessarily beneficial. For example, their use on the ceiling in the case considered in the previous section would probably only move the locus of the plume instability lower down from the ceiling. It appears preferable to assess the benefit of fins in retrospect rather than trying to model them.

2) The energy input to the bay frames can be adjusted so that the frames are hotter than the floor, and the ceiling can be made hotter than the floor. The main objective in doing this is to try to establish a stably stratified gas state in which there is ultimately little or no convection motion. This is the primary subject addressed in this section.

3) Use of a stainless steel structure in Fig. 2 is a prime factor in determining the homogeneity projected in the previous section. The temperature defect on the vertical walls will obviously be less if the structure is made of copper. In this section attention will continue to be restricted to stainless steel. The final foil support design, which has a copper hibachi, will be discussed in Sec. V.

Vertical Wall Temperature

Setting up a rigorously correct model for the situation envisaged in this subsection is quite an undertaking. Furthermore, it doesn't appear that useful to be rigorous since the purpose of this study was to establish plausibility of design concepts. They can be proved experimentally if adequate flexibility is allowed. Plausibility can be established with a simpler and highly idealized treatment. The essential features are that the bay frames are again treated as perfect reflectors and radiation is modeled using a locally one-dimensional or strip method. Given that the bay frames are not perfect reflectors nor uniformly heated, that the foil support temperatures vary from one support to the next as well as along each support, and that the ceiling and floor temperatures can

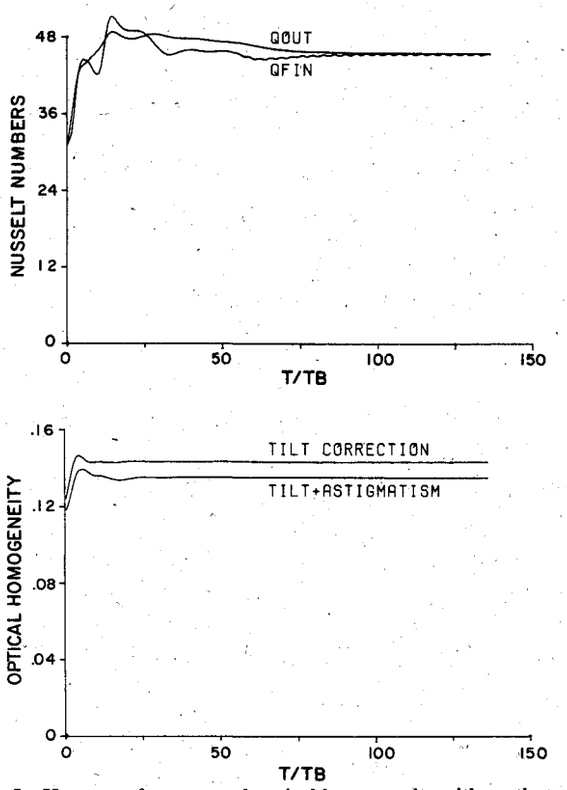

Fig. 5 Heat-transfer rates and optical homogeneity with no thermal grading.

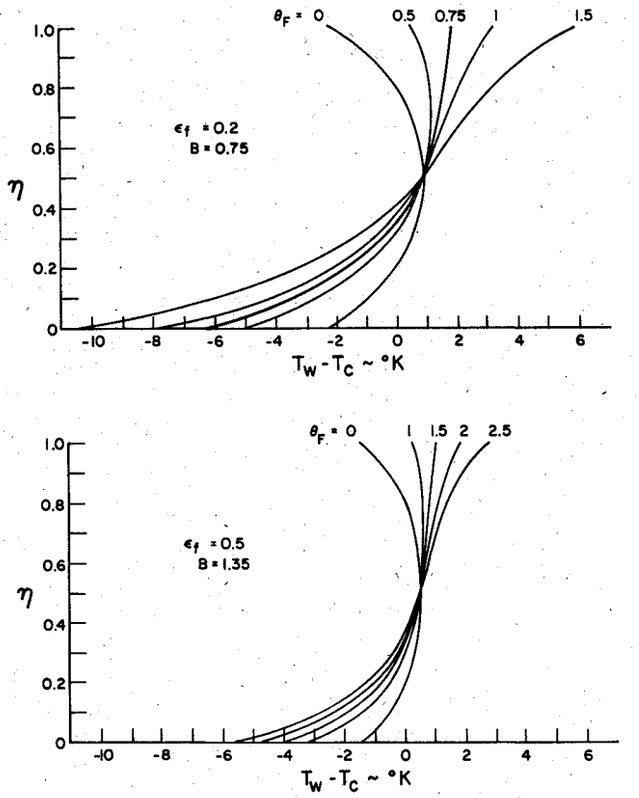

Fig. 6 Wall temperature distributions with thermal grading.

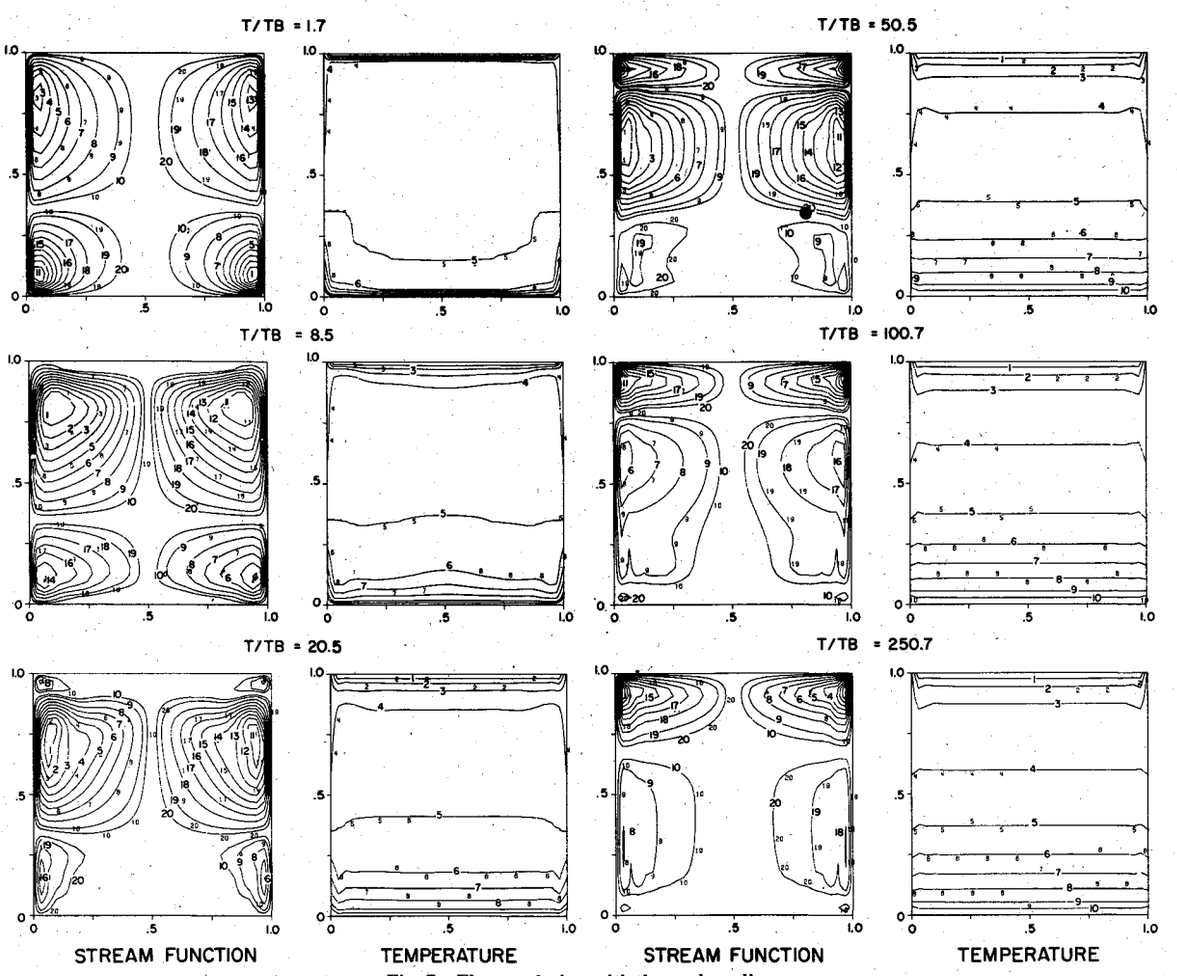

Fig. 7 Flow evolution with thermal grading.

be significantly different from the mean cavity temperature, the degree of idealization should be evident.

A steady-state conduction equation for the vertical bay frames will be required. Consider the top view of a bay in Fig. 2. Integration over a bay frame (i.e., a cross-hatched region) leads to

$$w_b h_b k_b \frac{d^2 T_b}{dy^2} = \alpha_s h_s \dot{Q}_{out} - w_b \dot{Q}_{in} \tag{18}$$

where $w_b = 0.95$ cm and $h_b = 1.35$ cm are the width and depth of the bay frame, y is the vertical coordinate, $\alpha_s = 0.2$ and $h_s = 2$ cm are the solidity and depth of the support bar hibachi, $\dot{Q}_{out}$ is the heat per unit solid area conducted into the hibachi, and $\dot{Q}_{in}$ is the heat input per unit frame area from the heating element. T_b should be understood to be the temperature of the bay frame where it contacts the primary foil. In all cases subscript b refers to the bay frames.

The normalized foil support bar temperature still follows from Eq. (10) and the linearized form for $\dot{Q}_R$ in Eq. (12) will again be used. Therefore,

$$\theta_s = 1 - (1+\theta_b)\cosh\left[\left(\frac{z}{L_s} - \frac{1}{2}\right)\sqrt{K}\right] \Big/ \cosh\left(\frac{1}{2}\sqrt{K}\right) \tag{19}$$

in this case, where K is defined in Eq. (13c) and θ_b is a normalized bay frame temperature,

$$\theta_b = (8\epsilon_f + 4\epsilon_r) T_c^3 (T_b - T_c) / \epsilon_r (T_c^4 - T_a^4) \tag{20}$$

The heat conduction equation for the bay frame then becomes

$$d^2\theta_b/d\eta^2 + A(B - \theta_b) = 0$$

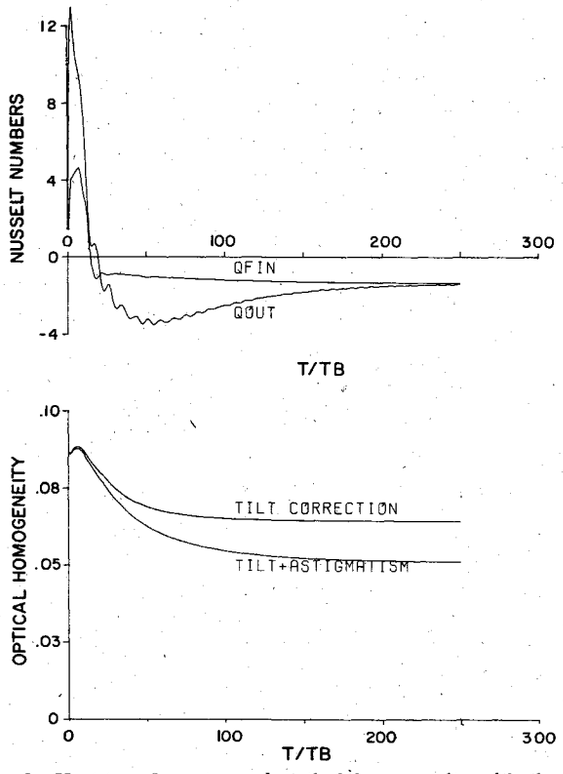

Fig. 8 Heat-transfer rates and optical homogeneity with thermal grading.

with

$$A = \frac{2\alpha_s h_s k_s H^2}{w_b h_b k_b L_s} \sqrt{K}\tanh\left(\frac{1}{2}\sqrt{K}\right)$$

$$B = \frac{w_b \dot{Q}_{in}/L_s}{\epsilon_r \sigma (T_c^4 - T_a^4)} \sqrt{K}\coth\left(\frac{1}{2}\sqrt{K}\right) \tag{21}$$

where $\eta = y/H$ and $H = 60$ cm is the cavity height. In the previous section the case of $B = 0$ and equal floor and ceiling temperatures (i.e., $\theta_b = 0$ on $\eta = 0,1$) was considered. This evidently leads to $\theta_b = 0$ everywhere and Eq. (19) reduces to Eq. (13a). The situation of interest in this section involves $B > 0$.

Achieving stable stratification requires the ceiling to be hotter than the floor. Care in notation will be required to avoid confusion. Define T_T to be the ceiling (or top) temperature, T_F to be the floor temperature, and set the mean cavity temperature $T_c = (T_T + T_F)/2$. Also,

$$\theta_F = (8\epsilon_f + 4\epsilon_r) T_c^3 (T_c - T_F) / \epsilon_r (T_c^4 - T_a^4) \tag{22}$$

Then the boundary conditions which will be used in solving Eq. (21) are $\theta_b = -\theta_F$ on $\eta = 0$ and $\theta_b = +\theta_F$ on $\eta = 1$. The solution for this general case is

$$\theta_b = B\left\{1 - \frac{\cosh[(\eta - \tfrac{1}{2})\sqrt{A}]}{\cosh(\tfrac{1}{2}\sqrt{A})}\right\} + \theta_F \frac{\sinh[(\eta - \tfrac{1}{2})\sqrt{A}]}{\sinh(\tfrac{1}{2}\sqrt{A})} \tag{23}$$

Conduction along the bay frame dominates for small A and θ_b approaches a quadratic form in that case.

The frontal area of the bay frame is small compared to the total frontal area of a bay (~4%). Therefore, to adequate approximation, the optical path-average temperature distribution on the vertical walls for this case follows from

$$\theta_w = \frac{1}{L_s}\int_0^{L_s} \theta_s dz = 1 - (1+\theta_b)\frac{2}{\sqrt{K}}\tanh(\tfrac{1}{2}\sqrt{K}) \tag{24}$$

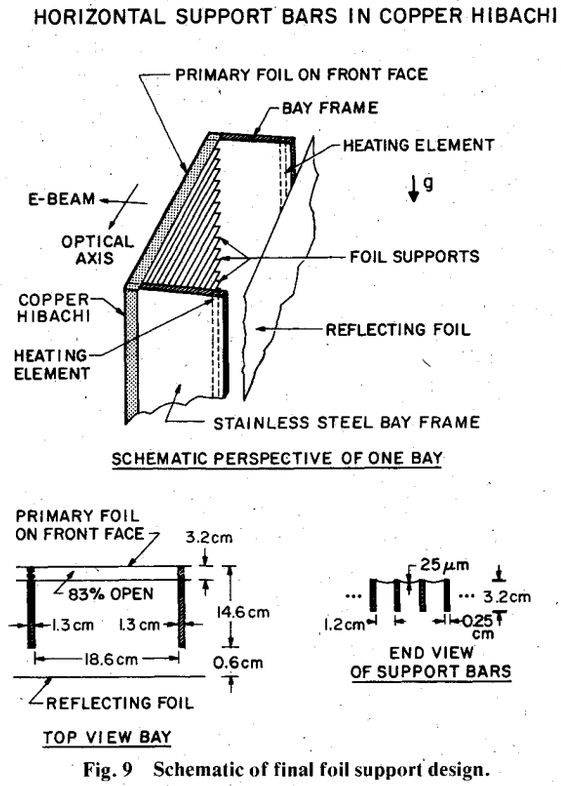

Fig. 9 Schematic of final foil support design.

In contrast to the previous section, θ_w is now a function of vertical position since $\theta_b = \theta_b(\eta)$. Temperature profiles are given in Fig. 6 for $T_c = 500$ K, $T_a = 300$ K, and $\epsilon_r = 0.03$ over a range of values of θ_F and for two values of the primary foil emissivity. The choices for the heat input parameter B are essentially arbitrary, though representative.

Note that there will generally be a temperature jump between floor and wall at $\eta = 0$ and between wall and ceiling at $\eta = 1$. For example, $B = \theta_F = 0.75$ and $\epsilon_f = 0.2$ involves $T_F - T_w(0) = 0.55$ K and $T_T - T_w(1) = 3.9$ K. This arises from two primary factors: the assumed good thermal contact of bay frames with the floor and ceiling and the use of horizontal foil support bars. If the ceiling is hotter than the floor ($\theta_F > 0$), the discontinuity at the lower juncture points ($\eta = 0$) is avoidable by setting $\theta_F = 1$ but the discontinuity at the upper juncture points ($\eta = 1$) is not avoidable. The temperature discontinuity at the wall-ceiling juncture has a deleterious effect on the medium homogeneity that can be achieved with thermal grading of the boundaries, as will be seen.

Numerical Simulation with Thermal Grading

The vertical wall temperature distribution will be based on the steady-state analysis discussed above. Parameter values $K = 5.37$ and $A = 18.0$ are chosen, corresponding to $T_c = 500$ K, $T_a = 300$ K, $\epsilon_r = 0.03$, and $\epsilon_f = 0.2$. Also, $B = \theta_F = 0.75$. The corresponding temperature profile is seen in Fig. 6. The nondimensional gas temperature $\theta = (T - T_F)/(T_T - T_F)$ will be used for the numerical simulation of natural convection. Boundary conditions are then $\theta = 0$ on $\eta = 0$, $\theta = 1$ on $\eta = 1$, and $\theta = (1 - \theta_w/\theta_F)/2$ on the vertical walls where θ_w follows from Eq. (24). $Gr = 2 \times 10^8$ and $Pr = \frac{2}{3}$ are adopted, as is appropriate for neon at 6 atm and 500 K, and $T_T - T_F = 11.4$ K. Initially, the gas is taken to be at rest and at the mean cavity temperature (i.e., $\theta = \frac{1}{2}$).

The evolution of the flow in a plane normal to the optical axis is displayed by the sequence of contour plots in Fig. 7. In the first frame the lower convection cells are strongest due to a greater differential between wall and initial gas temperature in those regions. At $t/t_B = 8.5$ the gas has begun to stably stratify around the cavity centerline and the upper set of convection cells are now stronger than the lower cells. Thereafter, the temperature discontinuity at the wall-ceiling junctures begins to assert itself. This takes time because gas below the ceiling heats up initially only by thermal diffusion. Convection ensues later because the gas in the diffusion layer falls after sufficient contact with the cooler vertical walls (and must be replaced to conserve mass). The temperature discontinuity at the floor-wall junctures is small compared to that at the ceiling so its effect is minor though evident at late times. As steady state is approached the dominant motion is in a layer near the ceiling.

Convection heat-transfer rates on the vertical walls (*QOUT*) and on the floor and ceiling (*QFIN*) are shown in Fig. 8. A plausible interpretation of negative values for $t/t_B \gtrsim 20$ is as follows. The convection cell induced by the temperature discontinuity at the wall ceiling junctures begins to build up around $t/t_B = 20$. It seems likely that this convection cell shields the ceiling from the lower 80-90% of the cavity gas, so that this lower gas primarily heat exchanges with the floor—a cooler boundary. On this basis the negative heat-transfer rates seen in Fig. 8 appear reasonable. Near steady-state heat transfer is achieved well before the end of this computer run.

A measure of optical homogeneity, $\delta\theta_{\text{rms}}$, is also given in Fig. 8. Here

$$\left(\frac{\delta\rho}{\rho}\right)_{\text{rms}} \sim \left(\frac{\delta T}{T}\right)_{\text{rms}} = \left(\frac{T_T - T_F}{T_c}\right)\delta\theta_{\text{rms}} \tag{25}$$

and the correction for astigmatism is in the vertical direction. In this case $\delta\theta_{\text{rms}} \sim 0.05 - 0.07$, $T_T - T_F = 11.4$ K, and $T_c = 500$ K, and so $(\delta\rho/\rho)_{\text{rms}} \sim 1.1 - 1.6 \times 10^{-3}$. This level of homogeneity is achieved within about 3 min. Note that this medium homogeneity is poorer than was found for equal floor, ceiling, and bay frame temperatures in the previous section. Although $\delta\theta_{\text{rms}}$ is less by a factor of two to three here, the ΔT used in nondimensionalization is larger by a factor of five. One can gain by correcting for even higher order aberrations. However, it is fairer to conclude that there is no advantage to thermal grading of the sort considered here so long as the bay frame is in good thermal contact with the ceiling. The possibility of designing for poor thermal contact between bay frame and ceiling seemed difficult and was not pursued.

It is evident that many closely spaced fins on the ceiling are not likely to help medium homogeneity in the laser cavity. They would probably do nothing more than move the effective locus of the ceiling-wall temperature jump farther down from the ceiling. It is possible that fins on the floor could improve medium homogeneity. The same can be said about the case considered in the previous section (cf. Fig 4). There tends to be motion down most of the vertical walls because they are relatively cooler, and the wall gas layers pass over the floor before returning up the central portion of the cavity. Fins on the floor would improve heat transfer to that gas before it rises in the central plume.

V. The Final Foil Support Design

The final foil support design is depicted in Fig. 9. The support bar hibachi is now a separate unit made of copper which sits on the front of stainless steel frames that form bays along the optical direction. Heating elements are embedded at the back of each bay frame as in Fig. 2. In addition to the use of copper, there are changes in dimensions between Figs. 2 and 9 which contribute to the projected excellent thermal uniformity in the final foil support structure.

It is convenient to think of the solid portion of the hibachi, seen in the top view of Fig. 9, as part of the bay frame. This is permissible provided a depth-average thermal conductivity k_b is used. Also, the thermal contact resistivity between two pieces of metal must be small. Equation (18) is then applicable and T_b is the bay frame temperature where it contacts the primary foil. Note that the copper segment of the bay frame will assure very uniform temperatures across the ends of the support bars. Equations (23) and (24) also hold here.

It is adequate to consider only the case of $B = \theta_F = 0$ to recognize the improvement in thermal uniformity that can result with the copper hibachi. Typical values are given in Table 3 for $T_c = 500$ K, $T_a = 300$ K, $\epsilon_r = 0.03$, and a range of primary foil emissivities. There is a question as to the validity of the simple modeling employed here to the level of thermal uniformity seen in Table 3. Moreover, the design problem has become one of achieving adequate thermal control with such tolerance. Demonstration that the final design will work will require experimentation and is beyond the scope of this paper.

A numerical simulation of cavity gas motion for the final design configuration has been performed and was reported in the original preprint version.[7] It was done for $B = \theta_F = 0$ and $T_c - T_w = 0.075$ K, corresponding to $\epsilon_f = 0.2$ in Table 3. To save space, only the conclusions of that study will be given here. The projected medium homogeneity at steady state is $(\delta\rho/\rho)_{\text{rms}} \sim 4 \times 10^{-5}$, which meets the goal given in Sec. I. As stated above, this is predicated on achieving adequate thermal control. Steady-state natural convection is expected after about 1.5 min elapsed time. Interestingly, the plume instability seen in Fig. 4 is not present at the lower Grashof number (1.4×10^6) appropriate for the copper hibachi.

VI. Conclusion

An attempt has been made in this paper to outline the inductive process involved in designing a sophisticated piece of apparatus. To keep the topic manageable the discussion has

Table 3 Combined radiation and conduction for final foil-wall design

	ϵ_f			
	1	0.5	0.2	0.2
K	0.568	0.288	0.120	0.064
$T_c - T_w \sim$K	0.072	0.074	0.075	0.076

been restricted to one particular aspect of a single-pulse excimer laser design and even then to a limited, although primary, phase of the thermal design for good cavity medium homogeneity. There is a problem with thermal homogeneity because other requirements on the laser system (acceptable e-beam losses, a cold e-beam cathode, and a hot cavity) lead to nonuniform heat losses through the boundaries of the cavity. Other arrangements would be preferable if thermal uniformity were the main goal. As it happens, however, the design choices available to achieve thermal homogeneity *are* limited by these other requirements.

The modeling itself is highly idealized, although complicated even still. In actual fact the natural convection is three-dimensional, there is interaction between convection and vertical wall temperature, and the radiative and conductive heat-transfer processes associated with the vertical wall are less simple. It is not appropriate to include all this detail at the design stage. Thus, a series of well-chosen idealizations are pursued to explore the main design considerations. The process is inductive and there is no guarantee that the examples chosen are definitive, just as there is no guarantee that all the relevant physics would be included in a sophisticated model of the "complete" problem.

There are two basic reasons that the final e-beam wall design is compatible with good laser cavity medium homogeneity. First, the heat loss rate through the hot vertical wall is substantially reduced by employing a secondary foil as a thermal radiation shield before the cold cathode. Second, the thermal conductivity of the cooper hibachi is relatively high compared to a relevant measure of the radiative loss. The effect of switching from stainless steel to a copper alloy is nicely illustrated by comparing Table 2 with Table 3. It is not resolved whether the projected medium homogeneity can actually be achieved because the problem is reduced only to the stage of defining requirements on a thermal control system for heater inputs. Designing the control system is not intrinsically difficult, but the tolerances involved are. This is something best assessed experimentally, with adequate flexibility designed into the system.

At the preliminary design stages it appeared obvious that grading the boundary temperature to produce an ultimately stably stratified gas state would be desirable. The example in Sec. IV shows that this is not necessarily true. Other studies not reported here show that thermal grading is useful in other circumstances. For example, closely spaced *vertical* foil support bars will involve minimal differences between optical path-average vertical wall and ceiling temperatures at their juncture. The main drawback of that arrangement is structural: a long span is involved. Use of fins to increase the ceiling area was also found to be detrimental in the situations considered, contrary to earlier beliefs. On the other hand, fins on the floor may be useful. The thermal design studies had to be reasonably sophisticated to resolve such subtleties.

Acknowledgment

The author wishes to express his thanks to John Boness, Jonah Jacob, and Jack Daugherty for many useful discussions during the course of this study. The work was supported by the Defense Advanced Research Projects Agency of the U.S. Department of Defense and was monitored by the U.S. Army Missile Command under Contract DAAK40-79-C-0197.

References

[1] Spiegel, E. and Veronis, G., "On the Boussinesq Approximation for a Compressible Fluid," *Astrophysical Journal,* Vol. 131, 1960, pp. 442-447.

[2] Trent, D. and Welty, J., "Numerical Computation of Convection Currents Induced by Fires and Other Sources of Buoyancy," Battelle Pacific Northwest Laboratories, Richland, Wash., Rept. WSCI 72-18, 1972.

[3] Knight, C. J., "Numerical Studies of Natural Convection in an Enclosure," Division of Engineering and Applied Physics, Harvard University, Cambridge, Mass., Tech. Rept. 15, 1975.

[4] Briley, W., "A Numerical Study of Laminar Separation Bubbles using the Navier-Stokes Equations," United Aircraft Research Laboratories, East Hartford, Conn., Rept. 5110614-1, 1970.

[5] Torrance, K., Orloff, L., and Rockett, J., "Experiments on Natural Convection in an Enclosure with Localized Heating from Below," *Journal of Fluid Mechanics,* Vol. 36, Pt. 1, 1968, pp. 21-31.

[6] Siegel, R. and Howell, J., *Thermal Radiation Heat Transfer,* McGraw-Hill, New York, 1972, Chap. 8.

[7] Knight, C. J., "Thermal Homogeneity in a Closed Excimer Laser Cavity," Paper 81-1132 presented at AIAA 15th Thermophysics Conference, June 1981.